Fluid Dynamics & Materials Processing
DOI:10.32604/fdmp.2020.09676
Article

A Combined Experimental and Numerical Study of Shotcrete Jets and Related Wet Spray Nozzles

Chang Su[1,2], Qiangqiang Zheng[3,*] and Wukun Zhao[4]

[1]State Key Laboratory of Mining Response and Disaster Prevention and Control in Deep Coal Mines, Huainan, 232001, China
[2]School of Mechanical Engineering, Anhui University of Science and Technology, Huainan, 232001, China
[3]School of Civil Engineering and Architecture, Anhui University of Science and Technology, Huainan, 232001, China
[4]State Key Laboratory of Safety and Health for Metal Mines, Maanshan, 243000, China
[*]Corresponding Author: Qiangqiang Zheng. Email: qqiangzheng@126.com
Received: 15 January 2020; Accepted: 19 August 2020

Abstract: In this research, the dynamics of wet spray nozzles with different geometries, used to accelerate shotcrete, are investigated on the basis of a suitable three-dimensional mathematical model and related numerical method. Simulations have been conducted in the frame of the SIMPLEC algorithm. The k-ε turbulence model has been used to account for turbulent effects. The study shows that when the angle of the convergent section is less than 3°, it has a scarce effect on the dynamics of the jet of shotcrete; with the increase of the convergence angle, the shotcrete jet velocity decreases and the nozzle wear increases; when this angle is greater than 6°, the concrete outlet jet velocity is very small and the nozzle can easily be blocked. Experimental results are in good agreement with the outcomes of the numerical simulations, which indicates that the used approach is reliable.

Keywords: Shotcrete; wet spraying nozzle; turbulence flow; convergence angle; numerical simulation

1 Introduction

Shotcrete or sprayed concrete, a cement-based mixture projected pneumatically in high velocities [1], is often used in various constructions, such as mine tunnels, railway and highway tunnels, and water conservancy culverts [2–4]. The flexibility of shotcrete makes it an effective alternative to conventional concrete in rock support, tunnel lining, and concrete repair. For example, the pneumatic projection allows shotcrete to be applied quickly on the uneven substrate surfaces, acting as excavation stabilization and arch lining in mines [5]. There is a problem of uneven injection and large amount of dust on the shotcrete construction site. Ulvestad et al. [6] ever indicated that mean exposures to total dust and respirable dust in shotcrete were significantly higher than in drillers (13.6, 3.4 mg/m^3 and 3.6, 1.2 mg/m^3). Georg et al. [7,8] compared the exposure situation of shotcrete dust in heading face between Swiss road tunnel and Munich subway tunnel with similar shotcrete and ventilation, results showed that the average fine dust concentration of road tunnel (13.2 mg/m^3) and subway tunnel (11.6 mg/m^3) was still higher in fact, what is more, the peak of dust concentration during shotcrete can reach up to more than 100 mg/m^3 for the

road tunnel and up to 70 mg/m^3 for the subway tunnel. Praml et al. [9,10] measured dust concentration during the shotcrete in amine tunnel construction site. Results showed that the fine dust concentration were 4.2 mg/m^3 for mixer operator and 11.6 mg/m^3 for nozzleman. The peak loads of dust concentration can reach up to five times the mean value. These problems not only waste valuable wet spray materials, generate a large amount of dust, damage the support strength, reduce work efficiency, but also pose a threat to the health and safety of workers.

Currently, when it comes to shotcrete, a large amount of researches pay their attention on the pumpability and shootability of fresh concrete [11–13] or the mechanism of sprayed concrete [14,15]. Chen et al. [16] summarized the technologies for reducing cement dust during shotcrete from new process, new apparatus to new materials, as well as the pathological damage of cement dust. Zeng et al. [17] indicated that the magnetized water can enhance the strength of shotcrete by 10% or so, and reduce the dust density by 50% in comparison with the ordinary shotcrete. The rebound rate of shotcrete mixed with magnetized water is greatly improved compared with that of the ordinary water shotcrete.

At present, there are few researches on the structure of wet spray nozzles, and in those researches the range of nozzle convergence angle is large lacking certain certainty, which has a great effect on the performance of nozzle [18]. This paper studies the effect of the shrinkage angle of the wet sprayer's nozzle on the uniformity of concrete injection and the reduction of dust through theoretical analysis, numerical calculation and experimental research. Based on the numerical calculation results, the specimen is made. The correctness of the numerical simulation results is verified in the experimental research and then applied to engineering practice.

2 Analysis and Calculation of Concrete Motion in Nozzle

2.1 Wet Sprayer Working Principle and Structure Characteristics of Nozzle

The construction of wet shotcrete refers to a process in which cement, water and aggregates are fully stirred in a certain proportion in blender, then pumped or air-conveyed to the nozzles, and finally, the concrete is accelerated with compressed air at the nozzle [19,20]. The nozzle as the concrete exit is essential to the whole machine. In order to improve the technology and product quality of the wet sprayer, it is necessary to study the influence of the nozzle structure on the concrete flow in the nozzle. The nozzle is composed of convergent section, mixed core, air-induction ring, and connection snap ring, as shown in Fig. 1, In practice, the compressed air and the accelerating agent enter the nozzle from the air induction ring (part 2 in Fig. 1). The concrete is pushed to the straight pipe (part 1) through the alternate delivery cylinder, and fully and evenly mixed in the material-gas mixing core (part 3) with high pressured air entering through the air induction ring (part 2). The suspended concrete particles pass through the front convergent section (part 5) and are sprayed from the outlet (part 6) to the sprayed surface, completing the entire concrete spraying operation.

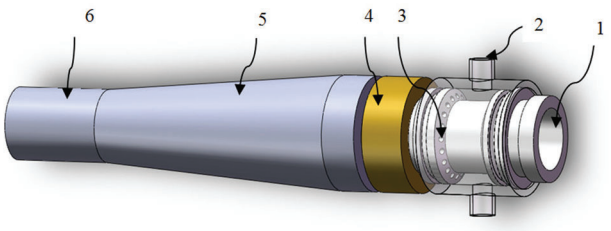

Figure 1: Diagram of nozzle structure

2.2 Mathematical Formulation

According to the working principle of the wet sprayer, the concrete mass is accelerated in the nozzle by the compressed air, and run in an axially-accelerated manner in the suspended state. At the same time, there is a circumferential rotational motion [21,22]. That is to say, the concrete mass is in a spiral motion in space and the axial and tangential forces are complex in the spraying process. However, the gravity and the levitation force balance each other in the vertical direction during the horizontal spray of concrete particles. The tangential force in the circumferential direction only produces a tangential rotational motion, without any effect on the axial movement of the concrete. Thus, the tangential force can be ignored when analyzing the axial movement of the concrete. The forces acting on the concrete mass mainly include the axial flow thrust F_R and the frictional resistance T of the nozzle inner wall. Fig. 2 briefly illustrates the forces on the concrete mass in horizontal pipes in dl section [23,24].

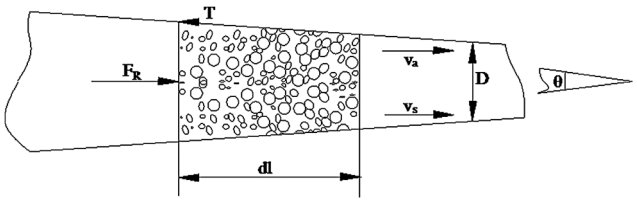

Figure 2: Force and motion diagram of concrete particle mass in horizontal conical tube

Airflow thrust Eq. (1):

$$F_R = C_s A_s \rho_a \frac{(v_a - v_s)^2}{2} \tag{1}$$

where C_s refers to the flow resistance coefficient; A_s is the total frontal area of concrete particle mass in dl section, m^2; ρ_a is the air density, kg/m^3; v_a, the air velocity, m/s; v_s, the transportation speed for concrete mass, m/s.

Pipe wall resistance Eq. (2):

$$T = \Delta P_l A = \lambda_s \frac{dl}{D} \rho_n \frac{v_s^2}{2} A \tag{2}$$

where λ_s refers to the resistance coefficient of concrete mass, and A is the cross section area.

Since:

$$\rho_n = \frac{q_{ms}}{A v_s} \tag{3}$$

$$C_s = C_n \left(\frac{v_n}{v_a - v_s}\right)^{\mathrm{k}} \tag{4}$$

According to the previous analysis, the airflow resistance of the shotcrete particles is within the Newton resistance zone, i.e., K = 0, thus it can be obtained:

$$C_n = g \frac{q_{ms}}{v_s} dl / \left(A_s \rho_a \frac{v_n^2}{2}\right) \tag{5}$$

Namely:

$$F_R = g\frac{q_{ms}}{v_s}gdl(\frac{v_a - v_s}{v_n})^{2-k} \tag{6}$$

$$T = g\frac{q_{ms}}{v_s}dl\frac{\lambda_s v_s^2}{2gD} \tag{7}$$

According to Newton's second law: $M_s\frac{dv_s}{dt} = F_R - T\cos\frac{\theta}{2}$, and combined it with Eq. (2):

$$\frac{1}{g}\frac{dv_s}{dt} = (\frac{v_a - v_s}{v_n})^2 - \frac{\lambda_s v_s^2}{2gD(\theta)} \tag{8}$$

where v_n stands for the suspension velocity, m/s; λ_s, flow resistance coefficient; D, inner diameter of the nozzle, mm; and θ, convergence angle of the convergent section, °.

The Eq. (8) is the differential equation of the motion of concrete mass in horizontal nozzle, which reflects the change of actual velocity of the concrete with time in the spraying process, that is, with the increase of time, the actual velocity of the concrete mass will accelerate from pumping speed to stable speed. The factors which affect the spray velocity of concrete include the convergence angle θ of the nozzle's convergent section, the suspension velocity v_n of the concrete mass, the airflow velocity v_a, and the flow resistance coefficient λ_s of the concrete mass. Among them, the convergence angle of the convergent section of the nozzle is crucial to the spray velocity of the concrete mass. The motion of the concrete flow in the nozzle can be described in this way. The concrete mass is pumped into the nozzle inlet, and under the action of high-pressure wind, the decelerating acceleration movement is performed. When the material mass acceleration is zero, the energy exchange between high pressure air and concrete mass ends. At that moment, the concrete mass gains the highest speed, and the material mass is in evenness motion.

The material mass can be considered to be an incompressible fluid due to neglecting the compressibility effects. The governing equations for the flow in the nozzle can be written as follow:

Continuity equation

$$\nabla \cdot v = 0 \tag{9}$$

Momentum equation

$$\rho\frac{\partial u_i}{\partial \tau} + \rho\frac{\partial(u_i u_j)}{\partial x_i} = -\frac{\partial p}{\partial x_i} + \frac{\partial \tau_{ij}}{\partial x_j} + \rho g_i + F_i \tag{10}$$

where ρ is the fluid density, kg/m^3; u_i, u_j are the fluid velocity of the unit body at the i and j direction respectively, m/s; p is the static pressure, Pa; τ_{ij} is the stress tensor, Pa; ρg_i are the gravitational body force, N/m^3; F_i is a momentum source term, N/m^3. In the calculation area, no external force is involved, thus the momentum source term $F_i = 0$.

3 Modeling and Numerical Simulation of Wet Sprayer Nozzle

3.1 Numerical Simulation and Boundary Condition

After the mesh is generated in ICEM®, the computational fluid dynamics (CFD) software ANSYS FLUENT® is used for numerical simulation. The whole nozzle is set up as a system of three-dimensional, incompressible, viscous, and turbulent flow with steady calculation. This research only focuses on the movement of the working medium, excluding the temperature change of the working medium, the

hydration reaction of the cement, and the change of the internal energy of the working medium. All the components of the nozzle are rigid, ignoring the deformation caused by the interaction between the solid wall forming the flow area and the working medium. The discretization scheme of the governing equation is first-order upwind scheme. SIMPLE solver is used to solve Pressure-Velocity Coupling. The Pressure Interpolation uses PRESTO! Scheme [25,26]. The max iteration number is 4000, and the convergence is assumed with all residues less than 10^{-5}.

The Operating environment is 101325 Pa; density of concrete particles is 2500 kg/m^3; concrete dynamic viscosity is 32 N·s/m^2; water-cement ratio is 0.48; thermal conductivity is 1.28 W/m°C; specific heat capacity is 970 J/(kg·K). The RNG k-ε model is more reliable and accurate than the standard k-ε model. What's more, since the high-pressure air supply process of the concrete pile mass is in the square area of turbulent flow resistance and the turbulence is a fully developed strong turbulent turbulence with large intensity, the RNG k-ε model is more suitable. Therefore, this study used the RNG k-ε turbulent model to resolve the flow equations [27,28].

Concrete inlet conditions is adjustable where the velocity boundary condition can be implemented. Considering the actual conditions of the wet sprayer, the spray capacity of wet sprayer is 7 m^3/h, and concrete flow direction is perpendicular to the nozzle inlet cross section, i.e., $u_y = u_z = 0$, $u_{\text{int\_concrete}} = u_x = 7/\pi D_1^2$, where D_1 refers to the nozzle inlet cross section. The hydraulic diameter is 64 mm. The air inlet boundary conditions, considering the practical operating conditions, are selected as the pressure inlet *pressure_inlet*. The air flow direction is perpendicular to the air inlet section of the nozzle mixing chamber, i.e., $u_y = u_x = 0$, $u_{\text{int\_air}} = u_x$. The field work wind pressure is 0.5 MPa [29], while the hydraulic diameter is 6 mm. The nozzle outlet boundary conditions are selected to be free outlet *Outflow*. The fluid Reynolds number and turbulence intensity can be solved with $Re = u_{\text{int}}\rho d/\gamma$ and $I = 0.16\ (Re)^{-1/8}$.

3.2 Geometry Model and Mesh Model of Nozzle Calculation Area

3.2.1 Geometry Model

The nozzle model is composed of a front convergent section, a middle mixing core, an air-induction ring, and a connecting ring, as shown in Fig. 1. The main parameters are listed in Tab. 1.

Table 1: Nozzle structure parameters

Nozzle parameters		Nozzle parameters	
Concrete inlet diameter D_1(mm)	64	Nozzle length L_1(mm)	595
Concrete outlet diameter D_2 (mm)	45	Convergence angle of convergent section θ(°)	4
Air inlet diameter D_3(mm)	6 × 20	Straight pipe of concrete inlet L_3(mm)	164
Air inlet declination β(°)	30	Straight pipe of concrete outlet L_4(mm)	100

3.2.2 Mesh Independence Study

The quality of mesh has great effects on the speed and accuracy of the simulation. The model adopts a hexahedral core meshing format at the inlet of the concrete and the outlet of the mixed fluid to improve the accuracy of meshing. Due to the presence of 20 high-pressure air inlets in the intermediate mixing chamber, the model structure is complex. Therefore, an unstructured grid division format is used to ensure a reasonable balance between calculation accuracy and computational resources. The computational domain mesh and mesh quality are presented in Fig. 3.

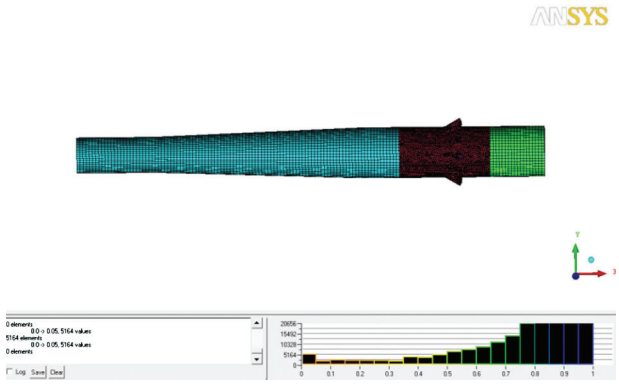

Figure 3: Diagrams of three mesh generation

The mesh independence of the model has been studied. The Max element of size 0.0010 m, 0.0015 m, 0.0020 m, 0.0025 m and 0.0030 m has been selected respectively for meshing, according to the meshing pattern mentioned above. When the cell size is 0.0030 m, the total of 738665 grid points are used to mesh the entire geometry. When the cell size is 0.0020, the total number of grid points is 1454508. When the cell size is 0.0010, the number of that is 2855213. Given that mean velocity of the outlet is an important comprehensive parameter, the mean velocity is chosen as the evaluation index. As shown in Fig. 4, when the number of grid points is more than 1.4 million, the rate of change of mean velocity is less than 0.5%. In this paper, the cell size is 0.0020 m. A total of 1454508 grid points are used to mesh the entire geometry.

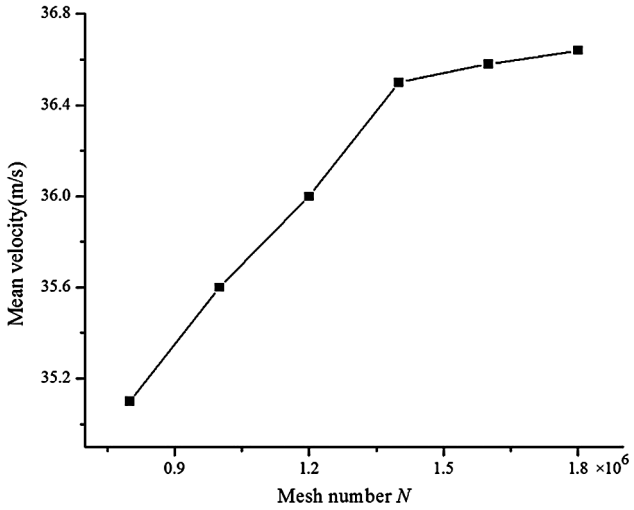

Figure 4: Mean velocity and grid number

4 The Effect of Convergency Angle on Wet Nozzle Performance

4.1 Numerical Calculation Results

In this study, modelling and numerical calculations were conducted with the convergency angles of convergent sections of 3°, 4°, 5°, 6°, and 7° respectively. Fig. 5 shows the flow velocity isogram when the convergency angle of convergent section θ is 4°.

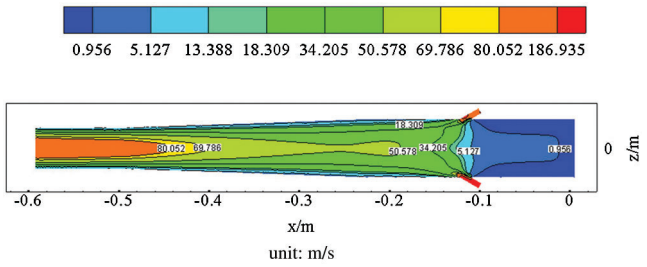

Figure 5: Velocity isogram on Y = 0 cross section

In the x = −0.595 outlet section, 11 collection points were selected in the Y-axis direction in an isometric way within the flow field boundary (−0.0225 m–0.0225 m), as shown in Fig. 6.

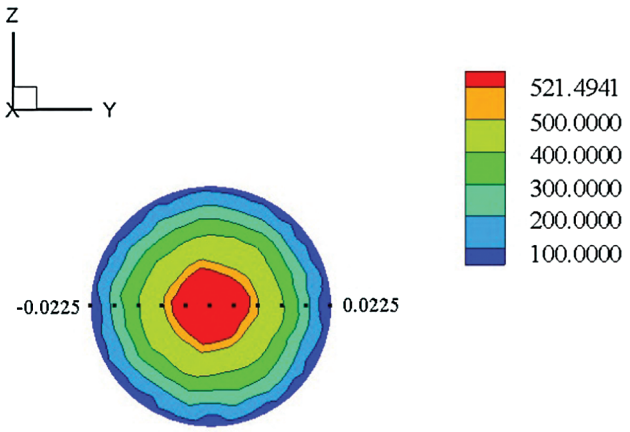

Figure 6: Collection points schematic diagram of x = 0.595 cross section

4.2 Analysis of Resultant Velocity of Outlet Section

Under the condition that the air pressure of the wet sprayer and the pumping pressure of the concrete are constant, the greater the outlet velocity of the concrete jet is, the less energy consumption of the contact between the concrete mass and the inner wall surface of the nozzle, and the small the wear of the nozzle will be. The average speed of the outlet section $\overline{U}$ (Eq. (11)) is regarded as an assessment index for the analysis of the outlet section velocity field, in the analysis of the average velocity of outlet section

$$\overline{U} = \frac{1}{N}\sum_{i=1}^{N} U_i \tag{11}$$

where U_i refers to the velocity of collection points in outlet section, m/s; and $\overline{U}$ is the mean velocity of collection points in outlet section, m/s.

Tab. 2 presents the mean velocity values of the outlet section collection points with various convergency angles of different nozzle models.

Import the mean data into Origin9® to fit the data curve, as shown in Fig. 7. It can be seen that when the convergence angle of the convergent section is less than 3°, it can be considered that the concrete mass is transported in an approximately equal straight pipe, and the concrete outlet speed does not change much;

when the convergence angle of convergent section is greater than 6°, the concrete transport velocity is very small and the nozzles are easily blocked.

Table 2: Mean velocity of outlet section collection points of different nozzle models

	Convergence angle (°)				
	3	4	5	6	7
Mean velocity (m/s)	40.64	37.70	36.47	35.40	19.66

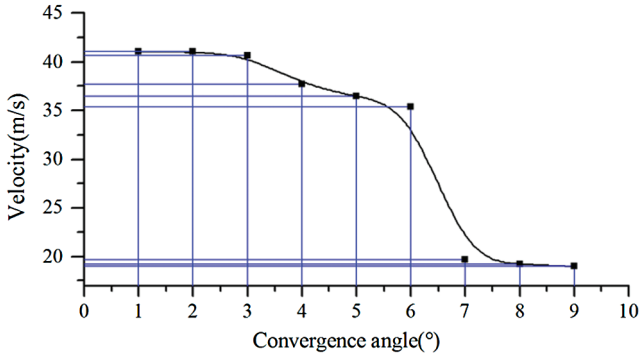

Figure 7: Mean velocity fitting curve of outlet section of different nozzle models

4.3 Analysis of Volume Fraction of Concrete Phase in Outlet Section

The distribution of the volume fraction of the concrete phase at the outlet of the nozzle is an important factor for judging the mixing effect of the nozzle structure on the mixed fluid. A reasonable distribution of the volume fraction of the concrete phase reflects the good mixing effect of the mixed fluid. In the past, the judgment of the mixing effect of the shotcrete flow can only be expressed indirectly based on the rebound rate of the sprayed wall surface. Through numerical simulation software analysis, the volume fraction of the concrete phase at the nozzle outlet of the mixed fluid is shown in Fig. 8.

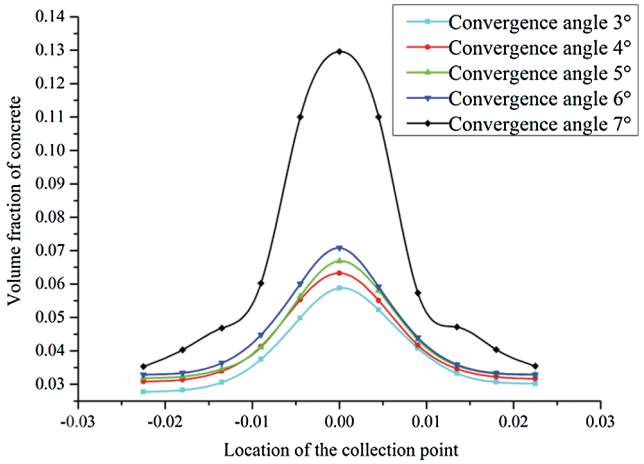

Figure 8: Volume fraction of the concrete phase in the outlet section x = −0.595 of different nozzle models

In order to objectively reflect the degree of mixing, both the standard deviation and the mean value are taken into account.

1. The degree of dispersion represents the ratio of the standard deviation to the measured mean value. The percentage expression is

$$R = \frac{S}{\bar{x}} \times 100\% \tag{12}$$

where S refers to the Standard deviation; and $\bar{x}$ is the arithmetic mean of volume fraction.

2. Evenness represents the degree to which a set of measurements approaches the mean value of the measurements. The mathematical expression is

$$H = 1 - R \tag{13}$$

The essence of dispersion and evenness is same, but just two different perspectives.

The analysis of the volume fraction of the concrete phase in the outlet section shows that both high concentration of concrete and low concentration fluctuation along the center of the nozzle are required in construction. Thus, suitable statistics to characterize this comprehensive evaluation index is necessary.

Define the comprehensive evaluation index Q as the product of the evenness and the measured mean values:

$$Q = \bar{x} \times H \tag{14}$$

From Tab. 3, it can be seen that the best sample of the outlet section concrete spray evenness is the model with the convergence angle of 6° in the convergent section.

Table 3: Concrete phase volume fraction analysis of outlet section

No.	Convergence angle (°)	Mean values (%)	Standard deviation (%)	Q value
1	3	3.82	1.08	2.73×10^{-2}
2	4	4.10	1.16	2.94×10^{-2}
3	5	4.24	1.24	3.00×10^{-2}
4	6	4.40	1.34	3.05×10^{-2}
5	7	6.48	3.45	3.03×10^{-2}

5 Experimental Study on Spraying Force Distribution Test of Shotcrete

5.1 Test System

Due to the limitation of test conditions, it is very difficult to directly measure the mixing quality of the concrete flow in the nozzle. Therefore, this study employed the method of measuring the impact force of the water jet flow abrasive on the object to indirectly determine the quality of the jet, and set up a shotcrete impact force distribution test system. Based on the field conditions of wet shotcrete as shown in Fig. 9, an effective concrete spray force distribution test scheme is proposed by using LabVIEW® to curve the input and output characteristics of the sensor, and analyzing and processing the test data [30].

Figure 9: Typical shotcrete spray

5.2 Sensor Layout

In order to measure the distribution of shotcrete impact force, a force transducer array system was designed. According to the characteristics of the central symmetrical structure of the shotcrete impact diffuse surface, taking into account the reduction of the test cost, 11 pressure transmitter collection points were arranged along a horizontal axis (−500 mm–500 mm) at a distance of 1000 mm × 1000 mm, as shown in Fig. 10, and fixed with nuts and the gaps were sealed with caulking glue. Collection points were evenly represented. The pressure transmitters in the array were numbered according to the distance from the centre of the bottom plate for the convenience of following test. From left to right, they were grouped by 0–10 in turn. The positions of 11 collection points in the coordinate system are No. 0 (−500, 0), No. 1 (−400, 0), No. 2 (−300, 0), No. 3 (−200, 0), No. 4 (−100, 0), No. 5 (0,0), No. 6 (100,0), No. 7 (200,0), No. 8 (300,0) No. 9 (400, 0), and No. 10 (500, 0).

Fig. 11 shows the assembly of the shotcrete test platform.

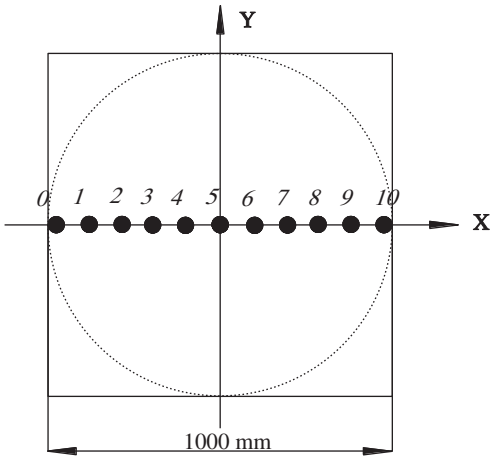

Figure 10: Sensor array distribution diagram

5.3 Nozzle Models Production and Testing

According to the previous analysis, the nozzle models with convergence angles of 4°, 5°, and 6° were fabricated as shown in Fig. 12, and field tests were conducted.

Fig. 13 shows the site of field test of shotcrete impact force test system.

Figure 11: Assembly of the Shotcrete test platform

Figure 12: Nozzle models

Figure 13: Field test

Setting LabVIEW, the sampling frequency is 1000, which means that it is collected 1000 times per second. Since the output signal of the transmitter is 0–5 V and the range is 0.5 MPa, the output pressure and voltage conversion formula is shown as Eq. (15).

$$P_{out} = \frac{V_{out}}{5} \times 0.5MPa \tag{15}$$

Multiple groups of test data have been obtained by replacing the convergent section to obtain. The test data are shown in Tab. 4.

Table 4: Mean values of test data of convergent section of different nozzle models

Collection point	Nozzle models (MPa)		
	4°	5°	6°
0	0.028224	0.029224	0.030264
1	0.030221	0.031171	0.032261
2	0.030931	0.031531	0.033331
3	0.032158	0.031898	0.035608
4	0.043221	0.044251	0.047961
5	0.051641	0.055231	0.059191
6	0.042998	0.045978	0.047088
7	0.032117	0.033807	0.034387
8	0.030873	0.031863	0.032123
9	0.029206	0.030226	0.030316
10	0.028128	0.029318	0.029398

The processed mean data was imported into Origin9® for data curve fitting, the results being showed in Fig. 14.

The distribution rule of the fitting curve is consistent with that of the volume fraction curve of the concrete phase of the nozzle outlet section shown in Fig. 8.

Based on the above analysis, Q values of nozzle models with different convergence angles in the convergent section were calculated, as showing in Tab. 5.

By calculating Q value of the comprehensive evaluation index, the nozzle model with convergence angle of 6° in convergent section and Q value of more than 5° and 4° has the best performed, which is consistent with the theoretical analysis and numerical calculation results. The nozzle model with the convergence angle of 6° in convergent section has good shotcrete evenness and the test results is satisfactory.

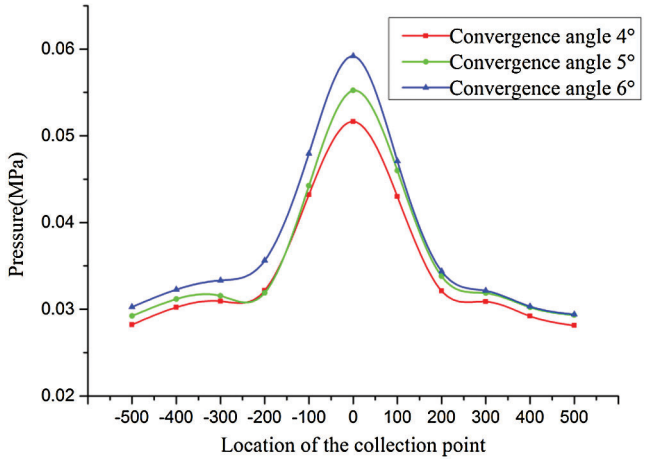

Figure 14: Mean test data curve of convergent section of different nozzle models

Table 5: Test data analysis of convergent section of different nozzle models

No.	Convergence angle (°)	Even value (MPa)	Standard deviation (MPa)	Q values
1	4	3.45×10^{-2}	3.03×10^{-5}	3.45×10^{-2}
2	5	3.59×10^{-2}	3.72×10^{-5}	3.58×10^{-2}
3	6	3.74×10^{-2}	4.64×10^{-5}	3.74×10^{-2}

6 Conclusion

In this study, the combination of numerical calculation and experimental research was employed to study the effect of the nozzle's convergence angle on the spraying performance of the concrete. According to the numerical calculation results, nozzle models were produced, and the shotcrete distribution test system was established to verify the numerical simulation, which then was applied to engineering practice. The study shows that when the convergence angle of the convergent section is less than 3°, the convergence angle has little effect on the shotcrete mass; with the increase of the convergence angle, the shotcrete mass jet velocity decreases and the nozzle wear increases; when the convergent section convergence angle is greater than 6°, the concrete outlet jet velocity is very small and the nozzle is easily blocked. The shotcrete impact force distribution test system was designed and assembled in line with the conditions of the wet shotcrete construction site, which can correctly collect the impact force of the sprayed surface and analyze the nozzle spray evenness. The test system provides an effective solution for on-site testing of the spraying performance of the wet sprayer nozzle. The force distribution test has a good consistence with the numerical simulation results.

Funding Statement: This work was financially supported by the Foundation of State Key Laboratory of Safety and Health for Metal Mines (2018-JSKSSYS-05).

Conflicts of Interest: The authors declare that they have no conflicts of interest to report regarding the present study.

References

1. Zheng, Q., Cheng, Y. H. (2019). Failure mechanism of different types of shotcrete based on modified Weibull distribution model. *Construction and Building Materials, 224,* 306–316. DOI 10.1016/j.conbuildmat.2019.07.071.
2. American Concrete Institute (2009). *506.5R-09: guide for specifying underground shotcrete*. Farmington Hills, MI: ACI.
3. Australian Shotcrete Society (2010). *Shotcreting in Australia*. Australia: Concrete Institute of Australia.
4. Martin, L., Seymour, B., Clark, C., Stepan, M., Pakalnis, R. et al. (2011). An analysis of flexural strength and crack width for fiber-reinforced shotcrete used in weak rock mines. *Transactions of Society for Mining, Metallurgy, and Exploration, 328,* TP09–TP062.
5. Höfler, J., Schlumpf, J. (2006). *Shotcrete in tunnel construction*, Putzmeister AG.
6. Ulvestad, B., Bakke, B., Eduard, W., Kongerud, J., Lund, M. B. (2001). Cumulative exposure to dust causes accelerated decline in lung function in tunnel workers. *Occupational and Environmental Medicine, 58(10),* 663–669. DOI 10.1136/oem.58.10.663.
7. Georg, P., Andrea, L. H., Richard, K., Günter, F. (1994). 31.O.06 Dust and shotcrete tunneling: did the exposure situation improve over the years? *Journal of Aerosol Science, 25(1),* 557–558. DOI 10.1016/0021-8502(94)90508-8.
8. Praml, G. J., Kessel, R. (1987). Continuous full shift personal dust exposure monitoring. *Journal of Aerosol Science, 18(6),* 911–914. DOI 10.1016/0021-8502(87)90154-6 .
9. Praml, G., Hartmann, A., Droz, P., Kessel, R., Fruhmann, G. (1995). Shotcrete in tunnel construction-the long-term development of exposure to dust. *Zentralblatt für Arbeitsmedizin, Arbeitsschutz und Ergonomie, 45(3),* 86–93.

10. Praml, G., Hartmann, A., Droz, P. O., Kessel, R., Knutti, R. et al. (1998). Dust exposure in shotcrete tunnelling. *Journal of Occupational and Environmental Hygiene, 4,* 455–464.
11. Chen, L. J., Liu, G. M., Cheng, W. M. (2016). Pipe flow of pumping wet shotcrete based on lubrication layer. *SpringerPlus, 5(1),* 8. DOI 10.1186/s40064-016-2633-3.
12. Ginous, N., Jolin, M. (2015). Investigation of spray pattern in shotcrete applications. *Construction and Building Materials, 93,* 966–972. DOI 10.1016/j.conbuildmat.2015.05.061 .
13. Liu, G. M., Chen, L. J. (2016). Development of a new type of green switch air entraining agent for wet-mix shotcrete and its engineering application. *Annual Review of Materials Science, 4,* 1–9.
14. Liu, G. M., Cheng, W. M., Chen, L. J. (2017). Investigating and optimizing the mix proportion of pumping wet-mix shotcrete with polypropylene fiber. *Construction and Building Materials, 150,* 14–23. DOI 10.1016/j.conbuildmat.2017.05.169 .
15. Wang, J. B., Niu, D. T., Zhang, Y. L. (2015). Mechanical properties, permeability and durability of accelerated shotcrete. *Construction and Building Materials, 95,* 312–328. DOI 10.1016/j.conbuildmat.2015.07.148 .
16. Chen, L., Li, P., Liu, G., Cheng, W., Liu, Z. (2018). Development of cement dust suppression technology during shotcrete in mine of China—a review. *Journal of Loss Prevention in the Process Industries, 55,* 232–242. DOI 10.1016/j.jlp.2018.07.001.
17. Zeng, X. T., Ren, Z. H., Wang, X. G. (2014). Experimental investigations on reducing the dust density and the rebound rate of shotcrete by using magnetized water. *Journal of China Coal Society, 39(4),* 705–712.
18. Lü, Z. B., Wang, Y., Liu, J. Q. (2015). Value of nozzle falloff angle of jet pump. *Journal of Jiangsu University: Natural Science Edition, 36(3),* 281–287.
19. American Concrete Institute (2005). *ACI 506R-05: Guide to shotcrete,* Farmington Hills, MI: ACI.
20. American Concrete Institute (2009). *ACI CP-60(09): Craftsman workbook shotcrete,* Farmington Hills, MI: ACI.
21. Bohnet, M., Wagenknecht, U. (1978). Investigations on flow conditions in gas/solid injector. *German Chemical Engineering, 1(5),* 298–304.
22. Bohnet, M., Teifke, J. (1985). New results on the efficiency of energy transformation in gas-solid injectors. *Reliable Flow of Particulate Solids, 3(5),* 1–18.
23. Ginouse, N., Jolin, M. (2014). Experimental and numerical investigation of particle kinematics in shotcrete. *Journal of Materials in Civil Engineering, 26(11),* 06014023–1–06014023–5.
24. Ginouse, N., Jolin, M., Bissonnette, B. (2014). Effect of equipment on spray velocity distribution in shotcrete applications. *Construction and Building Materials, 70,* 362–369. DOI 10.1016/j.conbuildmat.2014.07.116.
25. Wang, Z. Y., Yuan, C. L., Yu, Y. L. (2011). The analysis of internal flow field in oil-gas separator. *Procedia Engineering, 15,* 4337–4341. DOI 10.1016/j.proeng.2011.08.814.
26. Okyar, K. (2004). The experimental and numerical analysis of turbulent flow pressure drop of helical square duct. *Pamukkale University Journal of Engineering Sciences, 10(2),* 283–289.
27. Tian, P., Huang, J., Shi, W., Zhou, L. (2019). Optimization of a centrifugal pump used as a turbine impeller by means of an orthogonal test approach. *Fluid Dynamics & Materials Processing, 15(2),* 139–151. DOI 10.32604/fdmp.2019.05216.
28. Dandani, M., Lepiller, V., Lepiller, A. (2018). Numerical visualizations of mixing enhancement in a 2D supersonic ejector. *Fluid Dynamics and Materials Processing, 14(1),* 23–37.
29. Ministry of Housing and Urban-Rural Development of People's Republic of China (MOHURD) (2016). Technical specification for app1ication of sprayed concrete. *China Architecture & Building,* JGJ/T372-2016.
30. Su, C., Guo, Y. C. (2016). Test system of shotcrete impact force distribution based on the conductive rubber. *Electronic Journal of Geotechnical Engineering, 21,* 2826–2836.